crystals

MDPI

Article

A Quantum Chemical Study of the Gas-Phase Reaction Pathways in Metal–Organic Chemical Vapor Deposition Growth of InAlN

Peng Su [1,*], Yukang Sun [2] and Lijun Liu [2]

[1] School of Information and Artificial Intelligence, Xi'an University of Architecture and Technology Huaqing College, Xi'an 710043, China
[2] School of Energy and Power Engineering, Xi'an Jiaotong University, Xi'an 710049, China
* Correspondence: supeng@xauat-hqc.edu.cn

Abstract

Based on quantum chemical theory, the gas-phase chemical cross-reaction pathways in metal–organic chemical vapor deposition of InAlN films have been investigated. First, calculations of the oligomerization reactions of Al and In amides were performed to investigate the relative difficulty of generating several dimers and trimers within this system. The elimination reaction pathways were then investigated. The final stable products of the polymers were analyzed from both thermodynamic and kinetic perspectives, and the propensities of the reaction pathways were assessed from the viewpoint of the reaction rates. The results indicated that in the gas-phase reaction pathways of InAlN grown by metal–organic chemical vapor deposition, the equilibrium temperature for the dimerization reactions lies between 960 and 1061 K, and above this temperature range, dimers cannot form. Trimer formation is unlikely during the InAlN growth process. At higher reaction temperatures, the oligomers tend to first undergo intramolecular elimination, losing two CH4 molecules to form intermediate products, which then react with NH3 via intermolecular elimination to yield stable products. At lower reaction temperatures, the tendency is for continuous intermolecular elimination with NH4 to generate stable, methyl-free products.

Keywords: InAlN; metal–organic chemical vapor deposition; density functional theory; gas-phase reaction

1. Introduction

The band gap of InAlN alloys is continuously tunable from 0.7 to 6.2 eV, corresponding to emission wavelengths from 2 μm to 200 nm, covering the deep ultraviolet to near-infrared spectral range and making InAlN alloys ideal materials for optoelectronic devices [1–3]. When the In content of InAlN is 17%, the a-axis lattice constant matches that of GaN, allowing this alloy to replace AlGaN as a laser cladding layer. This alleviates the tensile stress to prevent crack generation, and because it has a larger refractive index difference with GaN than AlGaN, the optical confinement is enhanced, improving the light emission efficiency [4,5]. For example, Malinverni et al. [1,5] studied designs based on InAlN cladding layers, enabling blue and green laser diodes to achieve low threshold currents. Simultaneously, the InAlN/GaN heterojunction interface can form a higher concentration of two-dimensional electron gas than the AlGaN/GaN heterojunction interface, making it suitable for preparing high-performance power electronic devices [6]. It can also be used to fabricate lattice-matched high-electron-mobility transistors, contributing to improving the performance and reliability of high-frequency millimeter-wave devices [7].

Check for updates

Academic Editors: Brelon J. May, Robert A. Makin and Karol Strzałkowski

Received: 22 June 2026
Revised: 23 July 2026
Accepted: 23 July 2026
Published: 26 July 2026

Copyright: © 2026 by the authors. Licensee MDPI, Basel, Switzerland. This article is an open access article distributed under the terms and conditions of the Creative Commons Attribution (CC BY) license.

It should be noted that the growth of high-quality InAlN material faces a challenging temperature dilemma [8,9]. InN and AlN, as the constituent materials of InAlN, have very different growth temperature requirements. InN decomposes above 450 °C, and it is suitable for growth in low-temperature environments. For instance, when InN thin films are grown by metal–organic chemical vapor deposition (MOCVD) technology, the InN epitaxial layer achieves the best results at 605 °C. As the temperature increases, the intensity of its band-edge luminescence peak weakens and gradually redshifts [10]. In contrast, AlN requires growth temperatures above 1100 °C to ensure crystal film quality. For example, growing 1.5 μm thick AlN by MOCVD at a single-substrate temperature of 1180 °C yields an atomically flat surface [11–13]. This significant temperature disparity results in an extremely narrow temperature window for InAlN growth, making it difficult to simultaneously meet the requirements of both AlN and InN during a single growth process. This readily leads to phase separation and compositional inhomogeneity in InAlN, severely hindering the preparation of high-quality InAlN thin films.

The chemical reaction pathways of III-nitride MOCVD growth have been extensively investigated. Through first-principle calculations and thermodynamic analysis, Manoel et al. [14] investigated the formation mechanism of InAlN core–shell nanorods, evaluating the characteristics of In- and Al-containing precursors. The gas-phase reaction pathways for InAlN include the individual reaction pathways of AlN and InN, as well as the cross-reaction pathway between AlN and InN. The gas-phase reactions for AlN and InN growth mainly include the pyrolysis pathway and adduct pathway. By a combination of experiments and numerical calculations, McDaniel et al. [15] investigated the pyrolysis of trimethylindium in He, H2, and D2, demonstrating that H2 participates in and accelerates trimethylindium pyrolysis. Zuo et al. [16,17] computationally analyzed radical-involved metalorganic vapor phase epitaxy reactions in the trimethylgallium/NH3/H2 system, determining the different reaction pathways for the radical-involved gas-phase reactions at various temperatures. Oligomerization and elimination pathways also exist. Through numerical simulation of reactor transport-reaction processes, Mihopoulos [18,19] found that oligomer formation is the main reason for the decrease in the thin-film growth rate with reduced pressure. They suggested that dimers are the main precursors for thin-film growth, while trimers are the main precursors for nanoparticles.

Previous studies have focused on the individual reactions of InN and AlN within InAlN, while less attention has been paid to their cross-reactions in oligomerization and elimination. In this study, we performed quantum chemical calculations of the reactions during MOCVD growth of InAlN. First, the oligomerization reactions of In and Al amides were considered, exploring the relative difficulty of generating several dimers and trimers within this system. The elimination reaction pathways were then considered. This paper presents three reaction pathways (intramolecular elimination, intermolecular elimination, and intramolecular followed by intermolecular elimination), using heterodimers and homodimers as examples. By comparing the free energy differences, reaction energy barriers, and reaction rate constants of each reaction at different temperatures, the final stable products of the polymers were investigated from both thermodynamic and kinetic perspectives.

Density functional theory (DFT) and ab initio molecular dynamics (AIMD) simulations are powerful theoretical tools for exploring gas-phase reaction mechanisms during the MOCVD growth of nitride materials [20]. DFT calculations can provide accurate thermodynamic and kinetic parameters, including Gibbs free energy changes and energy barriers, to identify favorable precursor reaction pathways. As a complementary method, AIMD simulations can capture the dynamic structural evolution and real-time stability of reaction intermediates under actual growth environments. These well-established theoretical approaches have been extensively used to study the reaction behaviors of nitride precursors

and provide a reliable theoretical basis for mechanism exploration. Based on the above research background, this work employs DFT calculations to systematically investigate the oligomerization and elimination reaction pathways in the MOCVD growth of InAlN.

2. Computational Models and Model Validation

Based on previous research findings [21], in this paper, we propose gas-phase reaction pathways for MOCVD growth of InAlN, including the oligomerization reactions of amides and the elimination reactions of oligomers. We focus on the cross-polymerization pathways of dimethylindium amide ($DMInNH_2$) and dimethylaluminum amide ($DMAlNH_2$), and the elimination pathways of the oligomers, as shown in Figure 1.

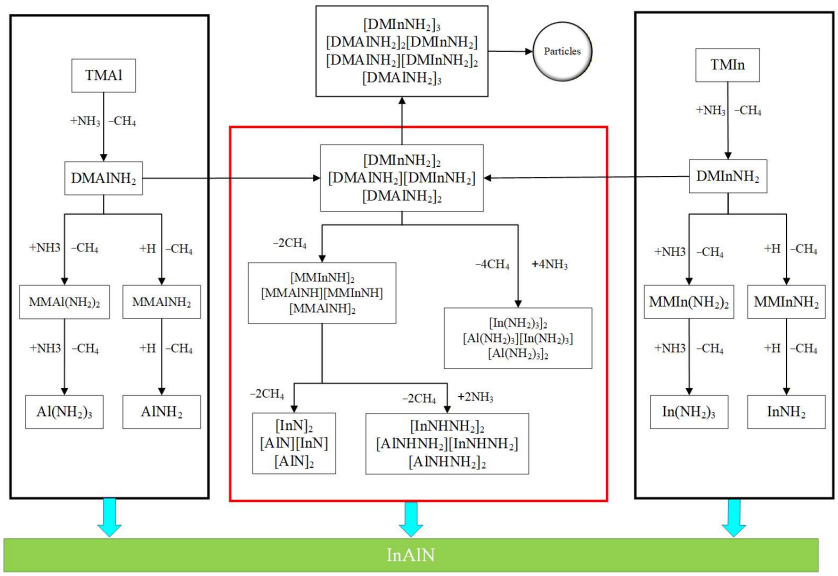

Figure 1. Schematic diagram of InAlN reaction pathways. The black boxes indicate individual reactions of Al and In, and the red box indicates the oligomerization and elimination pathways. This paper focuses on the oligomerization and elimination pathways.

The density functional theory (DFT) calculations were performed with the Gaussian09 program package [22]. The geometry optimizations, frequency calculations, and single-point energy calculations of the reactants, transition states, and products involved in the above reaction pathways were all performed using the B3LYP exchange–correlation functional within DFT [23]. For the geometry optimization and frequency calculations, the H, C, N, and Al atoms were treated with the 6-31G(d) basis set. For the In atom, the core electrons were treated with a pseudopotential, and the valence electrons were treated with the SDD basis set. For the transition states, the TS and QST2 methods in Gaussian09 were used to obtain the optimized structures and frequencies. To ensure that the obtained transition state connects the reactants and products, intrinsic reaction coordinate calculations were performed [24]. The post-optimization frequency calculation files, single-point energy, frequency scaling factor (taken as 0.9804), temperature, and other parameters were input into the Shermo program [25] to calculate the free energy.

It should be noted that no dispersion corrections were included in the present calculations. It is worth clarifying that dispersion interactions lead to minor deviations in the absolute stabilization energies of organometallic clusters and transition states. Nevertheless, the energy shifts originating from dispersion forces are approximately uniform for all intermediates and transition states along a given reaction pathway. This does not alter the relative barrier heights among distinct reaction channels, the identification of favorable reaction pathways, or the temperature-dependent evolution profiles of Gibbs free energy.

Consequently, the core mechanistic conclusions derived from the qualitative analysis in this work are not compromised by the exclusion of dispersion corrections. In addition, a substantial number of existing first-principles studies focusing on gas-phase oligomerization of III-nitride MOCVD precursors have adopted the uncorrected B3LYP functional. The computational parameters used in this work are consistent with those widely accepted in comparable mainstream research, which guarantees the cross-comparability of our results. For follow-up studies aiming at accurate quantitative evaluation of cluster binding energies, dispersion-corrected functionals such as B3LYP-D3 can be utilized.

To analyze the spontaneity and relative rate of each chemical reaction, we calculated the Gibbs free energy of all species at various temperatures. The relative reaction tendency was evaluated using the Gibbs free energy difference ΔG between reactants and products, where ΔG < 0 corresponds to a thermodynamically spontaneous reaction. For multi-step reactions at different temperatures, the relative reaction rate was assessed via the activation free energy ΔG* between the reactants and the transition state; a smaller ΔG* signifies a faster reaction. A schematic diagram of the reaction free energy change is shown in Figure 2. The reactants ultimately generate C through three steps. Because the free energy sequentially decreases from the reactants to B (i.e., ΔG < 0) and increases from B to C (i.e., ΔG > 0), the final reaction product is B.

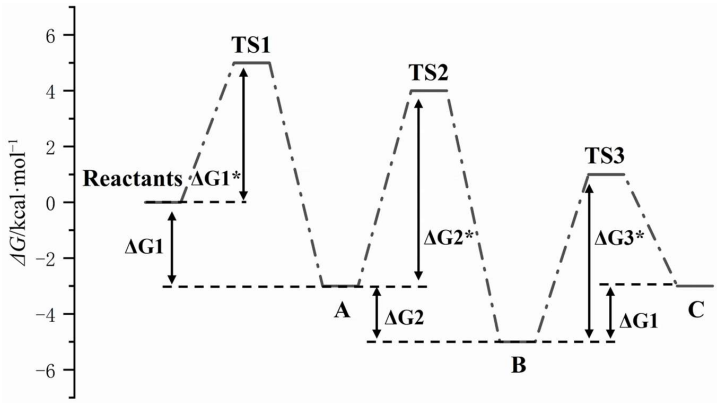

Figure 2. Schematic diagram of the reaction free energy change.

The calculated results of $DMXNH_2$ and $[DMXNH_2]_2$ (X = In or Al) are compared with literature data to validate the reliability of our computations. As listed in Table 1, the optimized structures obtained in this study agree well with literature results.

Table 1. Comparison of optimized amide bond lengths (Å) and bond angles (degrees).

Molecular Formula	Computational Method	X-N	X-C	Reference
$DMAlNH_2$	B3LYP/LANL2DZ	1.79	1.97	[21]
	B3LYP/def2-TZVPP	1.78	1.96	[26]
	B3LYP/6-31G(d)	1.79	1.97	This Paper
$DMInNH_2$	B3LYP/Lanl2dz	1.98	2.15	[27]
	B3LYP/In:3-21G(d,p)&AKR4C, H, N:6-311G(d,p)	2.06	2.20	[28]
	B3LYP/6-31G(d)/SDD	2.01	2.16	This Paper
$[DMAlNH_2]_2$	B3LYP/def2-TZVPP	1.98	1.97	[26]
	B3LYP/6-31G(d)	1.99	1.98	This Paper
$[DMInNH_2]_2$	B3LYP/6-311G(d,p) +SDD	2.22	2.15	[29]
	M062X/6-31G(d)/LanL2DZ	2.21	2.15	[30]
	B3LYP/6-31G(d)/SDD	2.23	2.16	This Paper

To further compare the relative speeds of different reactions under identical conditions, it is necessary to obtain the chemical reaction rate constant for each reaction. The chemical reaction rate constant is the key kinetic parameter describing the rate of a chemical reaction, and it is commonly denoted by the symbol k. Its magnitude directly reflects the reaction speed, with a larger k value typically indicating a faster reaction rate. It can be quantitatively related to important factors, such as the temperature and activation energy, through the Arrhenius formula, serving as the fundamental data for chemical engineering design, reaction control, and kinetic studies. Tian [31] compiled a set of Excel spreadsheets for calculating chemical reaction rate constants, enabling relatively convenient calculation of k. The calculated k values are used to compare the speeds of different reactions.

3. Results and Discussion

3.1. Oligomerization Reactions of $DMInNH_2$ and $DMAlNH_2$

In amides, the presence of lone pair electrons on the coordinating atom after bonding with the central atom results in strong chemical activity, making them prone to form oligomers [21], including dimers and trimers. Among these oligomers, dimers are the main precursors for thin-film growth, while trimers are the main precursors for nanoparticles.

Dimerization reactions include the formation of homodimers through oligomerization of $DMInNH_2$ or $DMAlNH_2$ individually, as well as the formation of heterodimers through co-oligomerization between $DMInNH_2$ and $DMAlNH_2$. The specific reactions are as follows:

$$2DMINNH_2 \rightarrow [DMINNH_2]_2 \quad (1)$$

$$2DMAlNH_2 \rightarrow [DMAlNH_2]_2 \quad (2)$$

$$DMINNH_2 + DMAlNH_2 \rightarrow [DMAlNH_2][DMINNH_2] \quad (3)$$

Reactions (1) and (2) are homodimerization, and reaction (3) is heterodimerization. All thermodynamic calculations in this work are carried out at a total pressure of 1 atm, which serves as the standard reference state for fundamental thermodynamic analysis and is widely adopted in theoretical studies of III-nitride gas-phase reactions. The free energy change diagrams for the dimerization reactions are shown in Figure 3, with the temperatures selected based on common InAlN growth temperatures (around 1000 K). For all three reactions, ΔG increases with increasing temperature, indicating that they are exothermic reactions with no energy barriers. For lower temperatures, ΔG is smaller, and the reaction proceeds more easily.

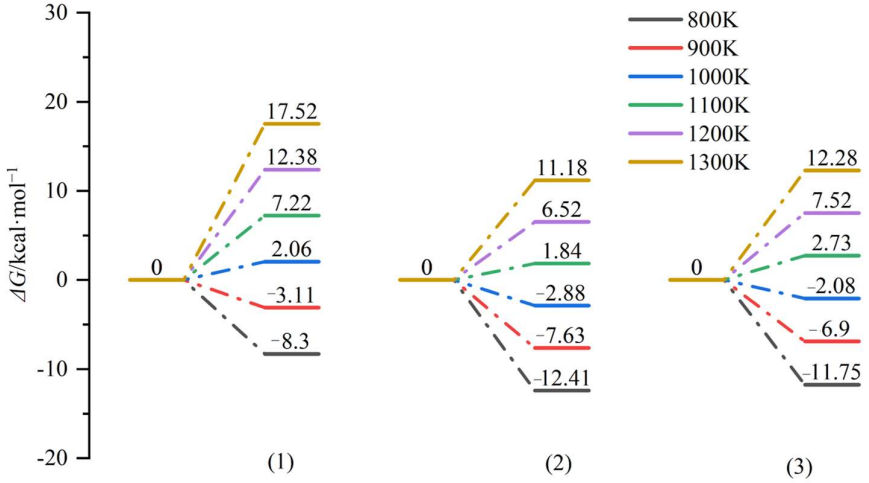

Figure 3. The free energy change diagrams for the dimerization reactions (1–3).

The equilibrium temperature for each reaction was estimated by linear interpolation, yielding the following three equilibrium temperatures: Te(1) = 960 K, Te(2) = 1061 K, and Te(3) = 1043 K. When the reaction temperature inside the reactor is lower than the corresponding equilibrium temperature, the amides will spontaneously generate dimers. Conversely, the dimers will spontaneously decompose. Comparing the three reactions at the same temperature (taking 900 K as an example), the ΔG values of reactions (1), (2), and (3) are −3.11 kcal/mol, −7.63 kcal/mol, and −6.9 kcal/mol, respectively. ΔG for reaction (2) is the lowest, and ΔG for reaction (1) is the highest, indicating that $[DMAlNH_2]_2$ is most easily formed, followed by $[DMAlNH_2][DMInNH_2]$ and $[DMInNH_2]_2$. This is because of the greater polymerization tendency of $DMAlNH_2$ than $DMInNH_2$, making it easier to oligomerize to $[DMAlNH_2]_2$ and $[DMAlNH_2][DMInNH_2]$.

Similar to dimerization, trimerization reactions also include the formation of homotrimers and heterotrimers, with heterotrimers having different formation pathways. The specific reactions are as follows:

$$[DMINNH_2]_2 + DMINNH_2 \rightarrow [DMINNH_2]_3 \quad (4)$$

$$[DMAlNH_2]_2 + DMAlNH_2 \rightarrow [DMAlNH_2]_3 \quad (5)$$

$$[DMINNH_2]_2 + DMAlNH_2 \rightarrow [DMAlNH_2][DMINNH_2]_2 \quad (6)$$

$$[DMAlNH_2]_2 + DMINNH_2 \rightarrow [DMAlNH_2]_2[DMINNH_2] \quad (7)$$

$$[DMINNH_2][DMAlNH_2] + DMINNH_2 \rightarrow [DMAlNH_2][DMINNH_2]_2 \quad (8)$$

$$[DMINNH_2][DMAlNH_2] + DMAlNH_2 \rightarrow [DMAlNH_2]_2[DMINNH_2] \quad (9)$$

The above trimers are all formed by the oligomerization of dimers with amides. Reactions (4) and (5) are homotrimerization, while reactions (6)–(9) are heterotrimerization. The free energy change diagrams for the trimerization reactions are shown in Figure 4. Similar to dimerization, ΔG increases with increasing temperature, indicating that the trimerization reactions are exothermic reactions with no energy barriers. For lower temperatures, ΔG is smaller, and the reaction proceeds more easily. However, within the selected temperature range, ΔG is consistently greater than 0, indicating that no trimers form within the InAlN growth temperature range.

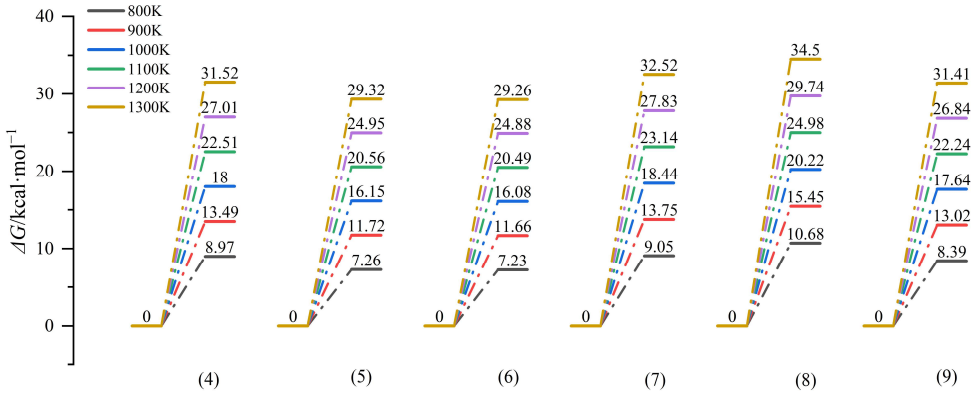

Figure 4. The free energy change diagrams for the trimerization reactions (4–9).

Taking 900 K as an example, the ΔG values of reactions 4–9 are 13.49 kcal/mol, 11.72 kcal/mol, 11.66 kcal/mol, 13.75 kcal/mol, 15.45 kcal/mol, and 13.02 kcal/mol, respectively. Comparing the ΔG values of the reactions at the same temperature, the ΔG values for reactions (5), (6), and (9) are slightly lower than those for reactions (4), (7), and (8). This is because the former three reactions involve $DMAlNH_2$, whose greater polymerization tendency makes the reactions proceed more easily.

If the InAlN reactor temperature is lowered to a temperature at which trimers can form, there are two reaction pathways for the $[DMAlNH_2][DMInNH_2]_2$ trimer: (6) and (8). Because ΔG for reaction (6) (13.75 kcal/mol) is lower than that for reaction (8) (15.45 kcal/mol) at the same temperature (e.g., 900 K), $[DMAlNH_2][DMInNH_2]_2$ tends to form by this pathway. Simultaneously, because ΔG for reaction (8) is higher than that for reaction (6), ΔG for its reverse reaction is lower, and $[DMAlNH_2][DMInNH_2]_2$ tends to decompose by the reverse reaction of pathway (8). Similarly, $[DMAlNH_2]_2[DMInNH_2]$ tends to form by reaction (7) and decompose by the reverse reaction of reaction (9).

The reactants and products of the dimerization and trimerization reactions are summarized, and the optimized structures of various species are shown in Figure 5. The Al–N bond length increases from 1.81 Å in the monomer to 2.00 Å in the trimer, and the In–N bond length increases from 2.01 Å in the monomer to 2.24 Å in the trimer. The Al–C and In–C bond lengths show slight increases from the monomer to the trimer. The Al–N bond length in $[DMAlNH_2]_2$ is 2.01 Å. In $[DMAlNH_2][DMInNH_2]$, the Al–N bond length shortens to 2.00 Å, while the In–N bond length increases from 2.23 Å in $[DMInNH_2]_2$ to 2.24 Å in [DMAlNH2][$DMInNH_2$]. In the heterodimer, the Al–N bond shortens and the In–N bond elongates owing to the mutual influence of Al and In. The same trend is observed in the trimers: compared with the homotrimers, the Al–N bond shortens and the In–N bond elongates in the heterotrimers.

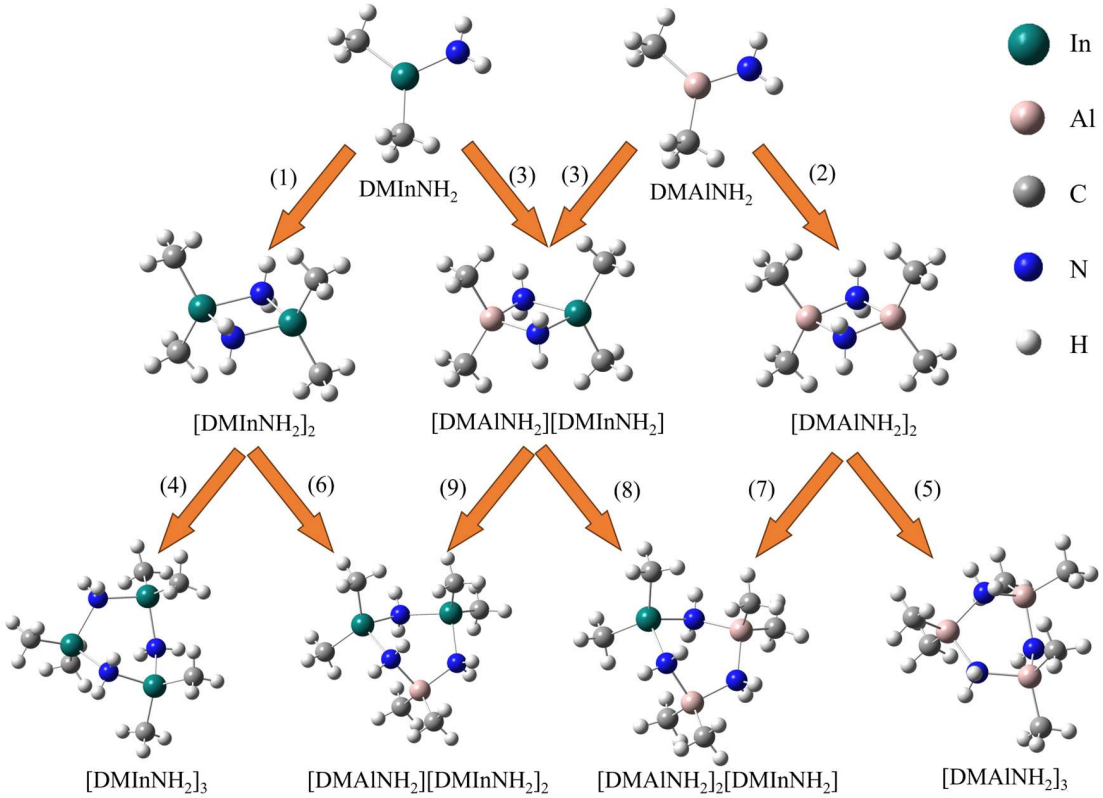

Figure 5. Optimized structures of the species involved in the oligomerization reactions, Numbers (1–9) denote the gas-phase reaction labels.

3.2. Elimination Reactions of the Oligomers

After amides form oligomers via oligomerization reactions, methane elimination occurs to generate stable products. The elimination reaction pathways are divided into three types: intramolecular elimination, intermolecular elimination with ammonia, and intramolecular elimination followed by intermolecular elimination. In this section, we report the results of quantum chemical calculations for these three pathways, using

[DMAlNH2][DMInNH2] as the starting material to calculate each reaction pathway and determine the final stable products of the oligomers.

3.2.1. Intramolecular Methane Elimination Pathway

Previous research [32] indicates that for homodimers ($[DMXNH_2]_2$) and homotrimers ($[DMXNH_2]_3$), the continuous methane elimination pathway can only proceed to the stable products $[MMXNH]_2$ and $[MMXNH]_3$ (MM = monomethyl). In this study, we used a similar research approach to study the intramolecular methane elimination pathway for hetero-oligomers. First, we assumed that the $[DMAlNH_2][DMInNH_2]$ oligomer undergoes a series of specific reactions for stepwise elimination of methane (CH_4) and the ultimate generation of [AlN][InN]. The feasibility of each elimination reaction used in the assumption was then individually verified. In the intramolecular methane elimination process of $[DMAlNH_2][DMInNH_2]$, the methyl groups on the metal atom and hydrogen atoms on the amino groups are removed and combine to form methane (CH_4). After multiple eliminations, [AlN][InN] is generated. The specific reactions are as follows:

$$[DMAlNH_2][DMINNH_2] \rightarrow [DMAlNH_2][MMINNH] + CH_4 \quad (10)$$

$$[DMAlNH_2][MMINNH] \rightarrow [MMAlNH][MMINNH] + CH_4 \quad (11)$$

$$[MMAlNH][MMINNH] \rightarrow [MMAlNH][INN] + CH_4 \quad (12)$$

$$[MMAlNH][INN] \rightarrow [AlN][INN] + CH_4 \quad (13)$$

The above reactions represent the intramolecular methane elimination pathway for the heterodimer. The reaction process involves an energy barrier. The optimized structures of the intermediate products and transition states obtained through quantum chemical calculations are shown in Figure 6. During methane elimination, the methyl group on the In atom is removed before that on the Al atom; the methyl groups on the X atom bearing more methyl groups are preferentially eliminated.

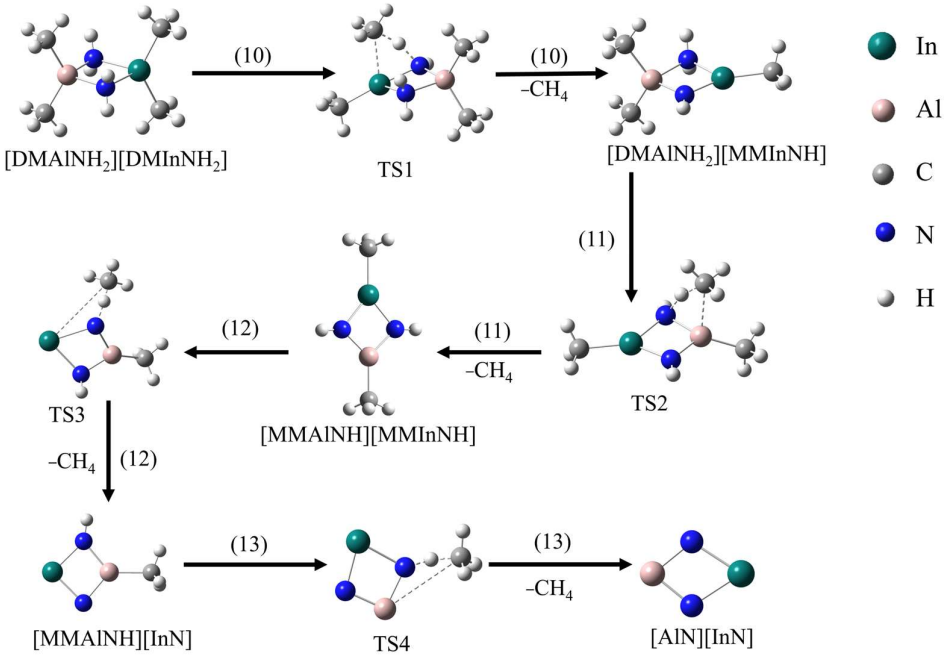

Figure 6. Optimized structures of the species in the intramolecular methane elimination pathway of $[DMAlNH_2][DMInNH_2]$, Numbers (10–13) denote the gas-phase reaction labels.

The free energy change diagram for this reaction pathway is shown in Figure 7. As the temperature increases, the ΔG values of the reactions decrease. By linear interpolation, the equilibrium temperature for reaction (10) is 849 K, meaning that when the reaction temperature exceeds 849 K, $[DMAlNH_2][MMInNH]$ spontaneously forms. For reaction (11), ΔG < 0 at all temperatures, indicating that the reaction proceeds spontaneously within the temperature range of 800–1300 K. For reactions (12) and (13), ΔG > 0 at all temperatures, meaning that reactions (12) and (13) do not proceed spontaneously. Among the reactants, intermediates, and final products, [MMAlNH][MMInNH] has the lowest free energy, indicating that it is more stable than the other species.

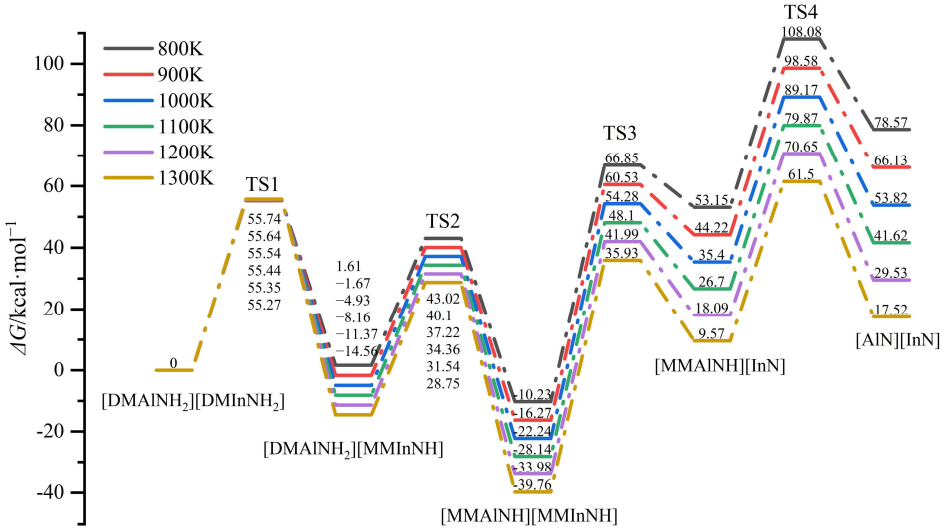

Figure 7. Free energy change for the intramolecular methane elimination reaction of $[DMAlNH_2][DMInNH_2]$.

3.2.2. Intramolecular Elimination Followed by Intermolecular Elimination Pathway

$[DMAlNH_2][DMInNH_2]$ first undergoes intramolecular elimination of CH4 to form [MMAlNH][MMInNH], followed by substitution of CH_3 by NH_3 to generate $[AlNHNH_2][InNHNH_2]$. The specific reactions are as follows: The first two reaction steps correspond to (10) and (11), and the subsequent reactions are as follows:

$$[MMAlNH][MMINNH] + NH_3 \rightarrow [AlNHNH_2][MMINNH] + CH_4 \quad (14)$$

$$[AlNHNH_2][MMINNH] + NH_3 \rightarrow [AlNHNH_2][INNHNH_2] + CH_4 \quad (15)$$

The optimized structures of the species along this reaction pathway are shown in Figure 8. During intramolecular methane elimination, the methyl group on the In atom is eliminated first, followed by that on the Al atom. During intermolecular methane elimination with ammonia, the methyl group on the Al atom is substituted first, followed by that on the In atom.

Reactions (10) and (11) are intramolecular elimination reactions, i.e., the first two steps of the intramolecular elimination pathway for $[DMAlNH_2][DMInNH_2]$. First, [MMAlNH][MMInNH] is generated after the removal of two methane molecules. Subsequently, intermolecular elimination with ammonia occurs, where ammonia molecules replace the methyl groups on the metal atoms, ultimately generating $[AlNHNH_2][InNHNH_2]$. The free energy change diagram for this pathway is shown in Figure 9.

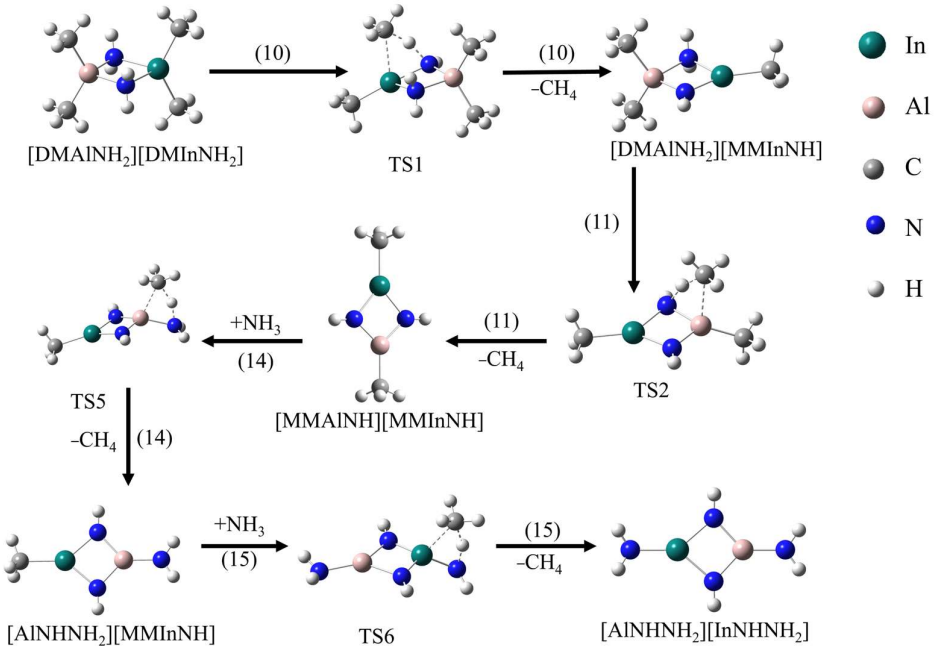

Figure 8. Optimized structures of the species in the intramolecular elimination followed by the intermolecular elimination pathway for $[DMAlNH_2][DMInNH_2]$, Numbers (10,11,14,15) denote the gas-phase reaction labels.

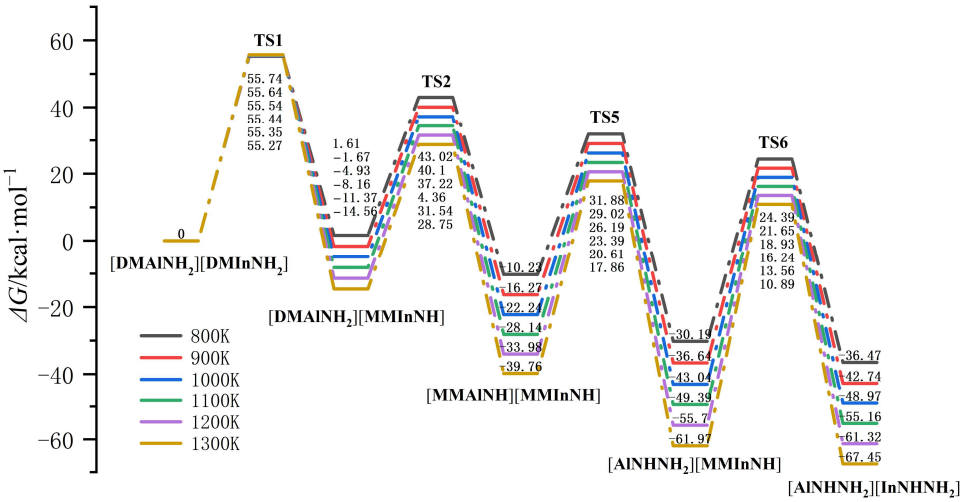

Figure 9. Free energy change for the intramolecular elimination followed by the intermolecular elimination pathway of $[DMAlNH_2][DMInNH_2]$.

At reaction temperatures above 849 K, the ΔG value for each reaction is less than 0, indicating that all of the reactions spontaneously proceed above 849 K, ultimately generating the stable product $[AlNHNH_2][InNHNH_2]$. As the reaction temperature increases, the energy barrier for each reaction shows an increasing trend, and the reaction rate slows, indicating that high temperatures inhibit the reaction.

3.2.3. Intermolecular Methane Elimination with Ammonia Pathway

In the intermolecular methane elimination reaction between $[DMAlNH_2][DMInNH_2]$ and ammonia, NH3 loses a H atom and continuously substitutes the CH_3 groups on the molecule. The displaced CH3 group then combines with H to form CH_4. The specific reactions are as follows:

$$[DMAlNH_2][DMInNH_2] + NH_3 \rightarrow [MMAl(NH_2)_2][DMInNH_2] + CH_4 \quad (16)$$

$$[MMAl(NH_2)_2][DMINNH_2] + NH_3 \rightarrow [MMAl(NH_2)_2][MMIN(NH_2)_2] + CH_4 \quad (17)$$

$$[MMAl(NH_2)_2][MMIN(NH_2)_2] + NH_3 \rightarrow [Al(NH_2)_3][MMIN(NH_2)_2] + CH_4 \quad (18)$$

$$[Al(NH_2)_3][MMIN(NH_2)_2] + NH_3 \rightarrow [Al(NH_2)_3][IN(NH_2)_3] + CH_4 \quad (19)$$

In this reaction pathway, each step involves the substitution of one methyl group by an amino group. The optimized structures of the species along this pathway are shown in Figure 10. First, the methyl group on the Al atom is substituted by an amino group, followed by that on the In atom; the methyl groups on the X atom bearing more methyl groups are preferentially substituted.

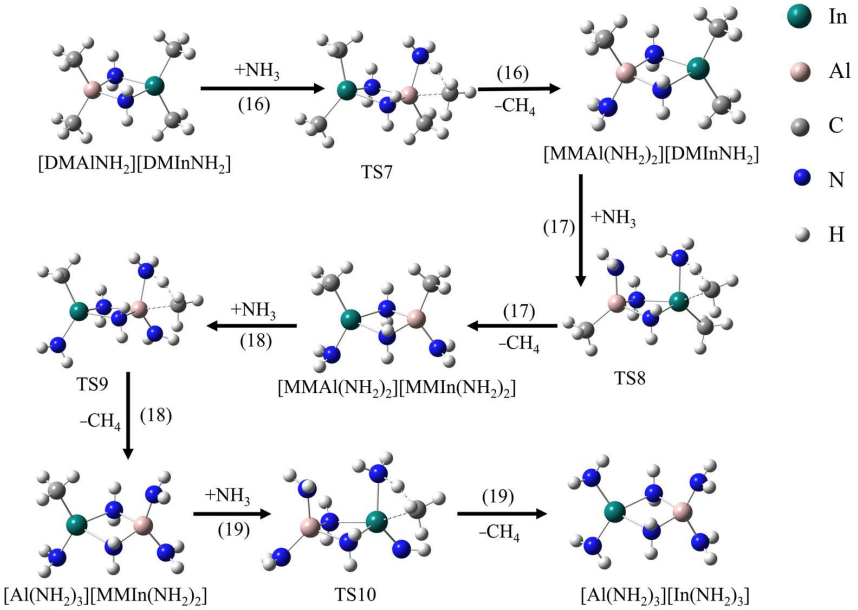

Figure 10. Optimized structures of the species in the intermolecular methane elimination pathway of $[DMAlNH_2][DMInNH_2]$ with ammonia, Numbers (16–19) denote the gas-phase reaction labels.

The free energy change diagram for this pathway is shown in Figure 11. The ΔG value for each reaction is less than 0, indicating that all of the reactions proceed spontaneously, ultimately generating the stable product $[Al(NH_2)_3][In(NH2)_3]$. As the temperature increases, the energy barrier for each reaction shows an increasing trend, and the reaction rate slows, indicating that high temperatures inhibit the reaction.

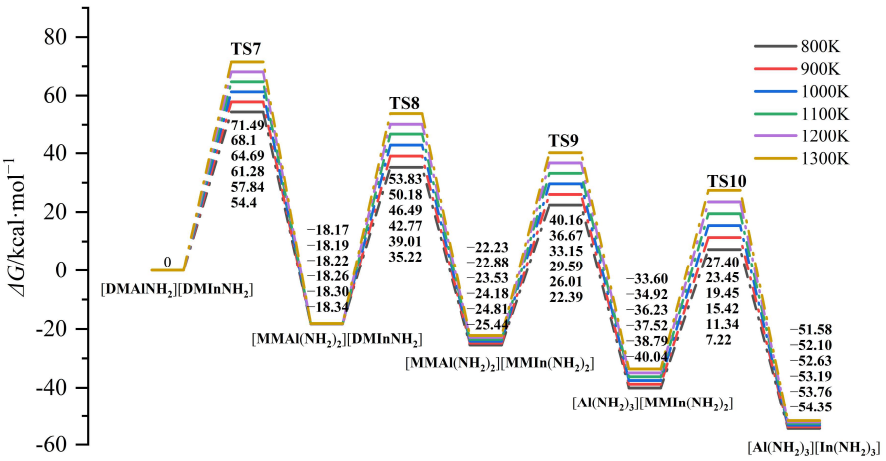

Figure 11. Free energy change for the intermolecular methane elimination reaction of $[DMAlNH_2][DMInNH_2]$ with ammonia.

3.2.4. Comparison of the Elimination Reaction Pathways

To determine which reaction is most likely to occur under different conditions, it is necessary to calculate the chemical reaction rate for each reaction and make a comprehensive judgment combined with the free energy change diagrams.

First, the reaction rate constants for the intramolecular elimination of [DMAlNH$_2$][DMInNH$_2$] and the intermolecular elimination of [DMAlNH$_2$][DMInNH$_2$] with ammonia were calculated at different temperatures (800–1300 K). The results are shown in Figure 12. When the temperature is above 850 K, the reaction rate constant for the intramolecular elimination of [DMAlNH$_2$][DMInNH$_2$] is higher than that for the intermolecular elimination of [DMAlNH$_2$][DMInNH$_2$] with ammonia; that is, the intramolecular elimination reaction is faster than the intermolecular elimination reaction. At 1000 K, the intramolecular elimination reaction rate constant is an order of magnitude higher than that of the intermolecular reaction, suggesting that intramolecular elimination predominates at this temperature.

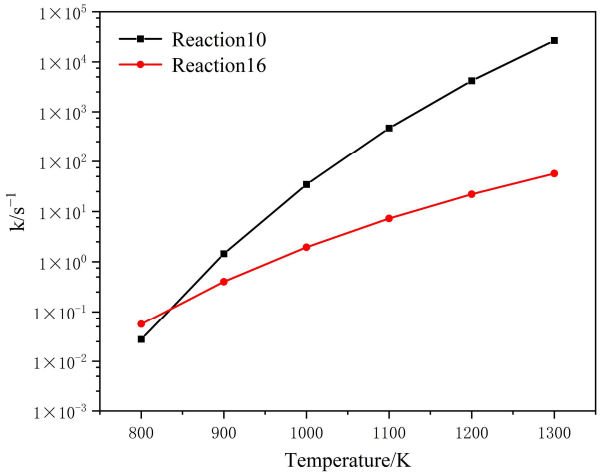

Figure 12. Comparison of the reaction rate constants (k) of reactions 10 and 16 at different temperatures.

Next, the reaction rate constants for the intramolecular elimination of [DMAlNH$_2$][DMInNH$_2$] and the pathway involving intramolecular elimination followed by intermolecular elimination with ammonia were calculated at different temperatures (800–1300 K). The results are shown in Figure 13. The solid lines indicate the first two steps of intramolecular elimination (reactions 10 and 11). The dashed lines indicate the continuation of intramolecular elimination (reaction 12) and intermolecular elimination (reaction 14). The rate constant of reaction 12 is significantly lower than those of the other three reactions at any given temperature, while the reaction rate constant of reaction 14 lies between those of reactions 10 and 11. This indicates that reaction 14 occurs at any temperature, corresponding to intramolecular elimination followed by intermolecular elimination.

In summary, for the intramolecular elimination pathway of In, Al-heterodimers, the reaction tends to generate [MMAlNH][MMInNH] and has difficulty proceeding further. For the intermolecular elimination pathway and the pathway involving intramolecular followed by intermolecular elimination, at higher temperatures, the reaction tends to proceed via reactions (10) → (11) → (14) → (15) to generate [AlNHNH$_2$][InNHNH$_2$]. These results are broadly similar to those reported by Sangiovanni et al. [33].

From the perspective of growth mechanism, the precursor reaction feasibility, intermediate stability, and energetic characteristics of products revealed in this work provide important guidance for the MOCVD growth of InAlN thin films. Existing studies have verified that for binary and ternary nitride systems fabricated via MOCVD, the stability of precursors and the energetic properties of various reaction intermediates and final products act as core factors governing the growth efficiency, micromorphology, and crystal quality

of thin films, which can directly determine the overall growth performance and device application potential of nitride films [14]. This rule is universally applicable to all types of III-nitride epitaxial growth systems, which further validates the scientificity and practicability of the gas-phase reaction mechanism and energy evolution law obtained by DFT calculations in this paper.

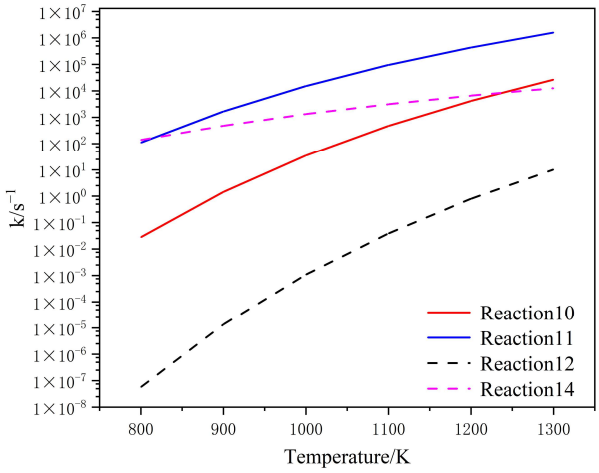

Figure 13. Comparison of the reaction rate constants for reactions 12 and 14.

4. Conclusions

The gas-phase reaction pathways in MOCVD growth of InAlN were investigated by DFT. The main conclusions are as follows:

(1) For the gas-phase reaction pathways of InAlN, oligomers may form at low temperatures and possibly decompose with rising temperature. $DMAlNH_2$ may possess a stronger polymerization tendency than $DMInNH_2$, so it is more likely to produce oligomers. Moreover, within the studied temperature window (800–1300 K), the ΔG values of trimerization reactions are consistently positive, which suggests that trimer species are unlikely to be generated under typical InAlN growth temperatures. It is probable that dimers are preferentially produced under such conditions.

(2) In the gas-phase reactions relevant to InAlN, oligomers yielded by oligomerization may further proceed via methane elimination processes. Three plausible elimination pathways were proposed and calculated in this work. At comparatively high reaction temperatures, oligomers are likely to first experience intramolecular elimination to produce $[MMAlNH_2][MMInNH_2]$; this intermediate may subsequently react with NH_3 through intermolecular elimination to yield the stable species $[AlNHNH_2][InNHNH_2]$. Under relatively low temperatures or high NH_3 partial pressures, intermolecular elimination may dominate, potentially generating $[Al(NH_2)_3][In(NH_2)_3]$.

Author Contributions: P.S.: writing—original draft, methodology, and investigation. Y.S.: writing—original draft, data curation. L.L.: supervision. All authors have read and agreed to the published version of the manuscript.

Funding: This research did not receive any specific grant from funding agencies in the public, commercial, or not-for-profit sectors.

Data Availability Statement: The original contributions presented in this study are included in the article. Further inquiries can be directed to the corresponding author.

Conflicts of Interest: The authors declare no conflicts of interest.

References

1. Luo, X.; Cui, P.; Linewih, H.; Cheong, K.Y.; Xu, M.; Chen, S.; Wang, L.; Sun, J.; Dai, J.; Xu, X.; et al. Influence of post fabrication annealing on device performance of InAlN/GaN high electron mobility transistors. *J. Phys. Chem. Solids* **2024**, *187*, 111870. [CrossRef]
2. Malinverni, M.; Castiglia, A.; Rossetti, M.; Ferhatovic, A.; Martin, D.; Duelk, M.; Velez, C. Blue and Green Low Threshold Laser Diodes with InAlN Claddings. *IEEE Photonics Technol. Lett.* **2023**, *35*, 1303–1306. [CrossRef]
3. Alam, S.N.; Zubialevich, V.Z.; Ghafary, B.; Parbrook, P.J. Bandgap and refractive index estimates of InAlN and related nitrides across their full composition ranges. *Commun. Mater.* **2020**, *3*, 16205. [CrossRef] [PubMed]
4. Du, F.; Jiang, Y.; Qiao, Z.; Wu, Z.; Tang, C.; He, J.; Zhou, G.; Cheng, W.-C.; Tang, X.; Wang, Q.; et al. Atomic layer etching technique for InAlN/GaN heterostructure with AlN etch-stop layer. *Mater. Sci. Semicond. Process.* **2022**, *143*, 106544. [CrossRef]
5. Malinverni, M.; Castiglia, A.; Rossetti, M.; Ferhatovic, A.; Martin, D.; Duelk, M.; Vélez, C. InAlN cladding implementation in green superluminescent diodes and lasers. *Appl. Phys. Lett.* **2023**, *122*, 201102. [CrossRef]
6. Alizadeh, M.; Tong, G.B.; Mehmood, M.S.; Qader, K.W.; Rahman, S.A.; Shokri, B. Band engineered Al-rich InAlN thin films as a promising photoanode for hydrogen generation from solar water splitting. *Sol. Energy Mater. Sol. Cells* **2018**, *185*, 445–455. [CrossRef]
7. Alvi, P.A. Enhanced optical gain characteristics of InAlN/δ-GaN/InAlN nanoscale-heterostructure for D-UV applications. *Superlattices Microstruct.* **2020**, *140*, 106450. [CrossRef]
8. Zhang, X.-Y.; Peng, D.-C.; Han, J.; Ren, F.-B.; Jiang, S.-C.; Tseng, M.-C.; Ruan, Y.-J.; Zuo, J.; Wu, W.-Y.; Wuu, D.-S.; et al. Effect of substrate temperature on properties of AlN buffer layer grown by remote plasma ALD. *Surf. Interfaces* **2023**, *36*, 102589. [CrossRef]
9. Wei, W.; Peng, Y.; Wang, J.; Saleem, M.F.; Wang, W.; Li, L.; Wang, Y.; Sun, W. Temperature Dependence of Stress and Optical Properties in AlN Films Grown by MOCVD. *Nanomaterials* **2021**, *11*, 698. [CrossRef] [PubMed]
10. Wu, J.; Walukiewicz, W.; Shan, W.; Yu, K.M.; Ager, J.W.; Li, S.X.; Haller, E.E.; Lu, H.; Schaff, W.J. Temperature dependence of the fundamental band gap of InN. *J. Appl. Phys.* **2003**, *94*, 4457–4460. [CrossRef]
11. Wang, G.; Zhang, L.; Wang, Y.; Shao, Y.; Chen, C.; Liu, G.; Wu, Y.; Hao, X. Effect of Temperature Gradient on AlN Crystal Growth by Physical Vapor Transport Method. *Cryst. Growth Des.* **2019**, *19*, 6736–6742. [CrossRef]
12. Nagamatsu, K.; Miyagawa, T.; Tomita, A.; Hirayama, H.; Takashima, Y.; Naoi, Y. High growth temperature for AlN by jet stream gas flow metalorganic vapor phase epitaxy. *Sci. Rep.* **2023**, *13*, 2438. [CrossRef] [PubMed]
13. Claudel, A.; Blanquet, E.; Chaussende, D.; Boichot, R.; Doisneau, B.; Berthomé, G.; Crisci, A.; Mank, H.; Moisson, C.; Pique, D.; et al. Investigation on AlN epitaxial growth and related etching phenomenon at high temperature using high temperature chemical vapor deposition process. *J. Cryst. Growth* **2011**, *335*, 17–24. [CrossRef]
14. Filho, M.A.M.; Hsiao, C.-L.; dos Santos, R.B.; Hultman, L.; Birch, J.; Gueorguiev, G.K. Self-Induced Core–Shell InAlN Nanorods: Formation and Stability Unraveled by Ab Initio Simulations. *ACS Nanosci. Au* **2022**, *3*, 84–93. [CrossRef] [PubMed]
15. McDaniel, A.H.; Allendorf, M.D. Autocatalytic Behavior of Trimethylindium during Thermal Decomposition. *Chem. Mater.* **2000**, *12*, 450–460. [CrossRef]
16. Zhang, H.; Zuo, R.; Zhong, T.; Zhang, L. Quantum Chemistry Study on Gas Reaction Mechanism in AlN MOVPE Growth. *J. Phys. Chem. C* **2020**, *124*, 2961–2971. [CrossRef] [PubMed]
17. Shi, J.C.; Zuo, R.; Meng, S.C. DFT study on adduct reaction paths of GaN MOCVD growth. *Sci. China Technol. Sci.* **2013**, *56*, 1644–1650. [CrossRef]
18. Mihopoulos, T. Reaction and Transport Processes in OMCVD: Selective and Group III-V Nitride Growth. Ph.D. Thesis, Massachusetts Institute of Technology, Cambridge, MA, USA, 1992.
19. Mihopoulos, T.G.; Gupta, V.; Jensen, K.F. A reaction-transport model for AlGaN MOVPE growth. *J. Cryst. Growth* **1998**, *195*, 733–739. [CrossRef]
20. An, J.D.; Dai, X.Y.; Zhang, Q.; Guo, R.; Feng, L. Gas-Phase Chemical Reaction Mechanism in the Growth of AlN during High-Temperature MOCVD: A Thermodynamic Study. *ACS Omega* **2020**, *5*, 11792–11798. [CrossRef] [PubMed]
21. Tang, L.; Zuo, R.; Zhang, H. Quantum chemical study on nanoparticles formation mechanism in AlGaN MOCVD growth. *J. Cryst. Growth* **2019**, *525*, 125201. [CrossRef]
22. Frisch, M.J.; Trucks, G.W.; Schlegel, H.B.; Scuseria, G.E.; Robb, M.A.; Cheeseman, J.R.; Scalmani, G.; Barone, V.; Petersson, G.A.; Nakatsuji, H.; et al. *Gaussian 09*; Gaussian, Inc.: Wallingford, CT, USA, 2009.
23. Lee, C.; Yang, W.; Parr, R.G. Development of the Colle-Salvetti correlation-energy into a functional of the electron density. *Phys. Rev. B* **1988**, *37*, 785–789. [CrossRef] [PubMed]
24. Becke, A.D. Density-functional thermochemistry. III. The role of exact exchange. *J. Chem. Phys.* **1993**, *98*, 5648–5652. [CrossRef]
25. Lu, T.; Chen, Q. Shermo: A general code for calculating molecular thermochemistry properties. *Comput. Theor. Chem.* **2021**, *1200*, 113249. [CrossRef]
26. Lisovenko, A.S.; Morokuma, K.; Timoshkin, A.Y. Initial gas phase reactions between Al(CH3)3/AlH3 and ammonia: Theoretical study. *J. Phys. Chem. A* **2015**, *119*, 744–751. [CrossRef] [PubMed]

27. Tzeng, Y.-R.; Raghunath, P.; Chen, S.-C.; Lin, C. Computational study of reaction pathways for the formation of indium nitride from trimethylindium with HN3: Comparison of the reaction with NH3 and that on TiO_2 rutile (110) Surface. *J. Phys. Chem. A* **2007**, *111*, 6781–6788. [CrossRef] [PubMed]
28. Cardelino, B.H.; Moore, C.E.; Cardelino, C.A.; Frazier, D.O.; Bachmann, K.J. Theoretical study of indium compounds of interest for organometallic chemical vapor deposition. *J. Phys. Chem. A* **2001**, *105*, 849–868. [CrossRef]
29. Lu, Z.; Pan, J.; Zhang, H.; Jiang, C.; Yang, W. Quantum chemical study of trimethylindium and trimethylgallium gas-phase reaction pathways in InGaN MOCVD growth. *J. Cryst. Growth* **2025**, *650*, 127992. [CrossRef]
30. He, X.; Xue, Y.; Zuo, R. Gas-Phase reaction mechanism of InN MOVPE: A systematic DFT study. *J. Cryst. Growth* **2023**, *612*, 127197. [CrossRef]
31. Lu, T. TSTcalculator. Available online: http://sobereva.com/310 (accessed on 21 June 2026).
32. Zhang, H. Study on Reaction Paths in GaN-MOVPE Growth by Computational Fluid Dynamics and Computational Chemistry. Ph.D. Thesis, Jiangsu University, Zhenjiang, China, 2017.
33. Davide, G.S.; Ricardo, F.; Gueorgui, K.G.; Anelia, K.G. Correction: Discovering atomistic pathways for supply of metal atoms from methyl-based precursors to graphene surface. *Phys. Chem. Chem. Phys.* **2023**, *25*, 5887. [CrossRef] [PubMed]

Disclaimer/Publisher's Note: The statements, opinions and data contained in all publications are solely those of the individual author(s) and contributor(s) and not of MDPI and/or the editor(s). MDPI and/or the editor(s) disclaim responsibility for any injury to people or property resulting from any ideas, methods, instructions or products referred to in the content.